PHYSICAL REVIEW B **89**, 045408 (2014)

Electron-photon scattering mediated by localized plasmons: A quantitative analysis by eigen-response theory

Kin Hung Fung,[1,2] Anil Kumar,[3] and Nicholas X. Fang[1,*]

[1]*Department of Mechanical Engineering, Massachusetts Institute of Technology, Cambridge, Massachusetts 02139, USA*

[2]*Department of Applied Physics, The Hong Kong Polytechnic University, Hong Kong*

[3]*Department of Electrical and Computer Engineering, University of Illinois at Urbana-Champaign, Urbana, Illinois 61801, USA*

(Received 15 January 2013; revised manuscript received 28 December 2013; published 13 January 2014)

We show that the scattering interaction between a high energy electron and a photon can be strongly enhanced by different types of localized plasmons in a nontrivial way. The scattering interaction is predicted by an eigen-response theory, numerically verified by finite-difference-time-domain simulation, and experimentally verified by cathodoluminescence spectroscopy. We find that the scattering interaction associated with dark plasmons can be as strong as that of bright plasmons. Such a strong interaction may offer new opportunities to improve single-plasmon detection and high-resolution characterization techniques for high quality plasmonic materials.

DOI: 10.1103/PhysRevB.89.045408 PACS number(s): 73.20.Mf, 68.49.Jk, 73.22.−f, 78.67.Bf

I. INTRODUCTION

The strength of the near-field resonant response of plasmonic nanostructures plays an important role in the processes of spontaneous emission [1–3] and stimulated emission [4–8]. Despite the rapid development of numerical simulation techniques, the strength of resonant response of an arbitrary plasmonic nanostructure is not easy to understand [9]. In particular, the scattering interaction strength between electron and photon mediated by plasmon resonance is nontrivial and, meanwhile, very crucial for high resolution microscopy and spectroscopy on plasmonic nanostructures.

Predicted by an eigen-response theory, dark plasmon modes [10–12] are considered to be weakly radiative plasmon modes in nanostructures which can give high gain factor in stimulated emission [4,7]. Research interest in dark plasmon modes and the associated Fano phenomena [13] has been growing rapidly due to many potential applications such as sensors, lasing, and nonlinear and slow-light devices [14–19]. Recently, dark plasmon modes have been observed in optical nanoantennas [20] using electronic excitation [21–24]. This presents great opportunity for using electron beam to study the local strength of high quality plasmonic resonances in spatial resolution smaller than 10 nm. More importantly, if electron-beam excited dark plasmon can be observed by means of photon detection such as in cathodoluminescence (CL) spectroscopy [25], it will give great advantages in imaging plasmonic nanostructures with simultaneous high spatial and spectral resolutions. However, far-field detection of energy from dark plasmons seems to be contradictory to their weak-radiation properties. It is thus our intention to study whether an electron can excite a dark plasmon with a strength that is strong enough to radiate enough photons for the detection in the far field.

In this paper, we use an eigen-response theory [11,26,27] to study the strong interaction strength of electron-photon scattering mediated by localized plasmons. The theory predicts a counterintuitive response from dark plasmon, which leads to a strong scattering interaction between a high energy electron and a photon. We use finite-difference-time-domain (FDTD) simulation and CL spectroscopy to verify the theoretical prediction by studying the scattering between electron and photon close to a plasmonic nanoantenna. The theoretical predictions agree with our CL experimental results.

The paper is organized as follows. We first describe our eigen-response theory and its prediction in Sec. II. Then, we present the verifications of the theoretical prediction by full-wave simulations in Sec. III A and experiments in Sec. III B.

II. EIGEN-RESPONSE THEORY

We first briefly introduce the prediction from the eigen-response theory. For a given excitation field $\mathbf{E}_{\text{exc}}(\mathbf{r},\omega)$, the general response polarization (dipole moment density) $\mathbf{P}(\mathbf{r},\omega)$ can be written as a linear combination of the eigenmodes $\mathbf{P}_j(\mathbf{r},\omega)$, where j is a label of one eigenmode. In an abstract-vector form, it is written as [27]

$$|P\rangle = \sum\nolimits_j \alpha_{\text{eig},j}|P_j\rangle\langle P_j|E_{\text{exc}}\rangle, \tag{1}$$

where $|P_j\rangle$ and λ_j ($\equiv \alpha_{\text{eig},j}^{-1}$) are, respectively, the jth eigenmode and the jth eigenvalue of an operator M which is defined in the relation between the excitation field $\mathbf{E}_{\text{exc}}(\mathbf{r},\omega)$ and the response $\mathbf{P}(\mathbf{r},\omega)$ through $M|P\rangle = |E_{\text{exc}}\rangle$ [28]. Since $\alpha_{\text{eig},j}$ has a dimension of polarizability, it is called eigen-polarizability [29] of the jth eigenmode. As we will see below, Eq. (1) suggests that a dark mode can contribute to a higher detected signal than a bright mode does in some situations, which seems to be contradictory to our usual belief.

To explain our prediction, let us consider a concrete example (bowtie nanoantenna). Dark modes can be formed in a system of coupled dipole resonators due to the hybridization among dipole modes [11], such as in bowtie nanoantenna [20]. The hybridization diagram for a bowtie nanoantenna formed by two equilateral Au triangles is shown in Fig. 1(a) for the dominant in-plane dipole modes in single triangles. It should be noted that the in-plane dipole modes in equilateral nanotriangle are degenerate. A simple derivation is given in Appendix A. When twofold degenerate dipole modes in each triangle

*nicfang@mit.edu

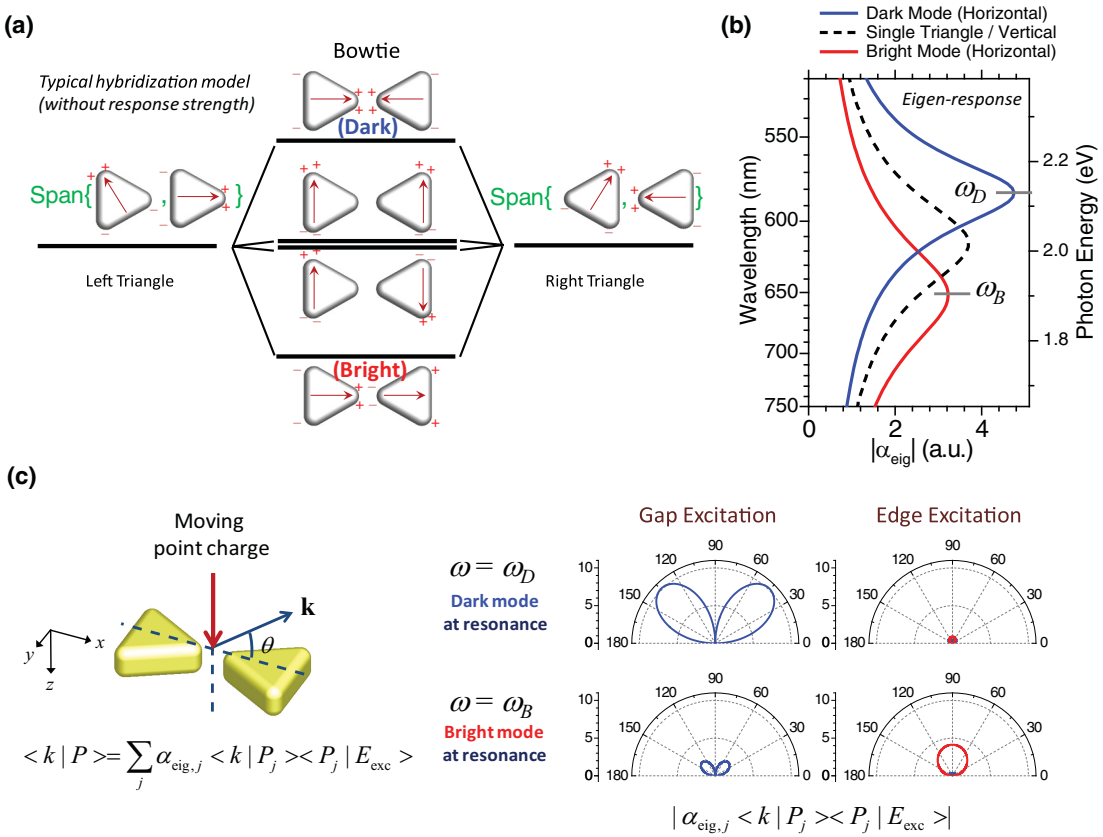

FIG. 1. (Color online) Demonstration of selection rule for CL. (a) Schematic diagram illustrating the hybridization between left and right particles, which form the dark modes in bowtie nanoantenna. "Span" indicates the degenerate space spanned by the dipole modes. (b) Magnitudes of the eigenpolarizabilities, α_{eig}, for the hybridized modes. The peaks indicate the resonant frequencies. (c) Predicted interaction strength between electron beam and photon as a function of angle θ. Blue (red) curve represents the contribution by the dark (bright) mode. The eigen-response theory predicts that the electron-photon scattering interaction strength mediated by dark plasmon can be higher than that of the bright plasmon mode. Units are arbitrary. Each Au particle has a tip-to-base size of 110 nm and thickness of 50 nm. The two Au particles are separated by a gap of 35 nm.

hybridize with the modes in the opposite triangle, there are four hybridized modes which include horizontal dark and bright modes indicated in Fig. 1(a) and the other almost degenerate vertical modes. The magnitudes of the eigenpolarizabilities, α_{eig}, for these plasmon modes are shown in Fig. 1(b) with their peaks indicating the resonant frequencies. The horizontal dark and bright modes are well separated in frequency, while the vertical modes are almost indistinguishable. In the following, we will focus on distinguishing the horizontal dark and bright plasmon modes. For a system that supports one dark mode $|P_D\rangle$ and one bright mode $|P_B\rangle$, the radiation amplitude (i.e., the interaction strength with free photon) is

$$\langle k|P\rangle = \alpha_{\mathrm{eig},B}\langle k|P_B\rangle\langle P_B|E_{\mathrm{exc}}\rangle + \alpha_{\mathrm{eig},D}\langle k|P_D\rangle\langle P_D|E_{\mathrm{exc}}\rangle, \quad (2)$$

where $\alpha_{\mathrm{eig},D}$ and $\alpha_{\mathrm{eig},B}$ are the eigenpolarizabilities of the dark mode and bright mode, respectively, and $|k\rangle$ is a plane wave with wave vector $\mathbf{k}$.

In general, $\langle k|P_D\rangle$ has a magnitude smaller than $\langle k|P_B\rangle$. However, a dark mode with higher quality factor should also have larger magnitude of α_{eig} at resonance [29]. As a result, the magnitude of $\alpha_{\mathrm{eig},D}\langle k|P_D\rangle$ can be comparable with $\alpha_{\mathrm{eig},B}\langle k|P_B\rangle$. In addition, a crucial factor that determines the ultimate radiation is the projection magnitudes $\langle P_B|E_{\mathrm{exc}}\rangle$ and $\langle P_D|E_{\mathrm{exc}}\rangle$. By choosing a zero projection to the bright mode, i.e., making $\langle P_B|E_{\mathrm{exc}}\rangle = 0$, we can have strong photon radiation dominated by the dark mode, which means a strongly enhanced interaction between electron and photon by dark plasmon. For an excitation by a high energy electron (30 keV), the final interaction strength predicted by the theory is shown in Fig. 1(c). The integrals for the projection magnitude for different positions are given in Appendix B. The intermediate steps in obtaining the final interaction strength are further explained in Appendix C.

III. VERIFICATIONS

To support our prediction, we performed FDTD simulations as well as experiments for the case of excitation by electron beam, which is considered to be a fine and controllable excitation source. In both our simulation and experiment, a 30 keV electron beam is incident normally to a bowtie nanoantenna. The three dimensional geometry of the bowtie antenna in our simulation is almost the same as in the experiment, except for the imperfection of the fabricated sample and the very thin ($\sim$3 nm) adhesion layer below Au particles.

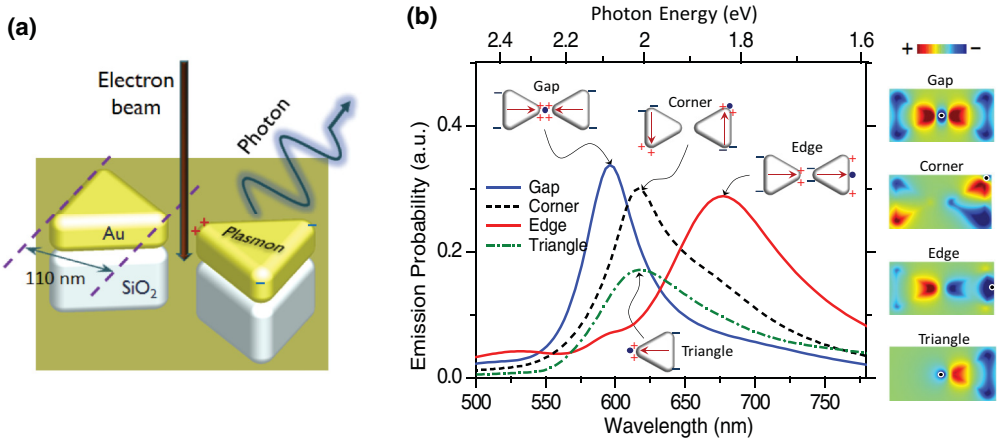

FIG. 2. (Color online) Numerical results on the scattering interaction strength between a 30 keV electron and a photon. (a) The rounded bowtie structure used in numerical simulations. Each Au particle is lifted away from the substrate by a 85 nm thick SiO_2 layer of the same shape. (b) Solid lines display the photon emission spectra for bowtie nanoantenna, which indicate the scattering interaction strength. Dash-dotted line displays the spectrum for single triangle. The diagrams next to spectral peaks indicate the position of electron beams and the corresponding plasmon modes excited by the beam. Colored plots on the right show the field patterns on a plane that is 2 nm above the surface of the nanoantennas. The color indicates the electric field normal to the monitored plane, which can approximately represent the surface charge density.

A. FDTD simulations

Figure 2(a) shows a schematic of the problem we consider. Electron beam is modeled in FDTD simulation as a moving point charge. Details of the simulation method can be found in Appendix D and elsewhere [30]. To match the fabricated sample, all corner and edges in the model structure have a rounding radius of 15 nm (see Supplemental Material [31]). We simulate and measure the photon emission for different fixed e-beam locations, which indicates the strength of the scattering interaction between electron beam and photon. Simulation results in Fig. 2(b) show that there is a dominant peak associated with each fixed e-beam. When the e-beam is fixed at the center (gap), right upper corner, and right edge of the bowtie antenna, we observe a peak at $\sim$600 nm, 620 nm, and 680 nm, respectively. We see that there are at least three different plasmon modes supported by the bowtie antenna. This is consistent with our prediction that four resonant modes are supported while two of the modes are almost degenerate such that they can hardly be distinguished. To further verify our theory and understand the peaks, we also simulate the case of single nanotriangle [dashed line in Fig. 2(b)]. Such a peak wavelength corresponds to the dipole resonance of single nanotriangle, while the peaks for gap, edge, and corner excitations correspond to antiparallel horizontal dipoles, parallel horizontal dipoles, and vertical dipoles, respectively. The above classification of peaks is verified by simulating the field patterns at the corresponding peaks in Fig. 2(b). The right colored panels in Fig. 2 show the z component of the electric field at a plane located 2 nm above the surface of the bowtie nanoantenna for the three dominant peaks. These patterns can approximately represent the surface charge density. We see that, when fixing e-beam at the central gap and observing the field pattern at the wavelength of 600 nm, the distribution of the induced charges is symmetric in x-direction, which represents a pair of antiparallel dipoles. For edge excitation at 680 nm, the induced charges show an almost antisymmetric distribution except the field produced by the e-beam itself near the right edge. For corner excitation at 620 nm, the induced charges show a pair of antiparallel vertical dipoles. This agrees with our theory that the vertical modes have wavelengths very close to the single triangle case. Apart from the dominant peak positions, we also see some small features at shorter wavelengths, which may correspond to higher order modes.

Here, we briefly discuss why both dark and bright modes can be selectively excited and analyzed in the far field with strong signals. When we fix the e-beam at the center of the gap, the excitation field produced by the e-beam has an azimuthal symmetry with respect to the center of the bowtie. Therefore, only the plasmon with charge distribution symmetric in both directions can be excited ($\langle P_D|E_{\rm exc}\rangle \neq 0$ and $\langle P_B|E_{\rm exc}\rangle = 0$) and this leads to a pure excitation of horizontal antiparallel dipole mode, which has the shortest wavelength among the three observable peaks. When the e-beam is fixed at the edge, a mirror symmetry is broken and the excitation of the horizontal parallel dipole mode is possible ($\langle P_D|E_{\rm exc}\rangle \neq 0$ and $\langle P_B|E_{\rm exc}\rangle \neq 0$). Since the e-beam is far away from the center of bowtie nanoantenna, it is more favorable to the excitation of horizontal parallel mode, which leads to a peak at the longest wavelength. Details of how each mode contributes to the total signal is illustrated in Appendix C. Similarly, in the case of e-beam fixed at the corner, the vertical in-plane dipole modes can be excited due to the broken mirror symmetry of the source in the y-direction.

To further demonstrate the roles of projected magnitudes $\langle P_j|E_{\rm exc}\rangle$, we repeat the simulation by changing the position of the electron beam from the gap to the edge. The results in Fig. 3 show the peak positions for different e-beam excitation locations are the same except the strength of signal, indicating a gradual change in projection magnitude from domination of anti-parallel mode to parallel mode (from "i" to "iv"). We see that there is no component of parallel mode contributing to

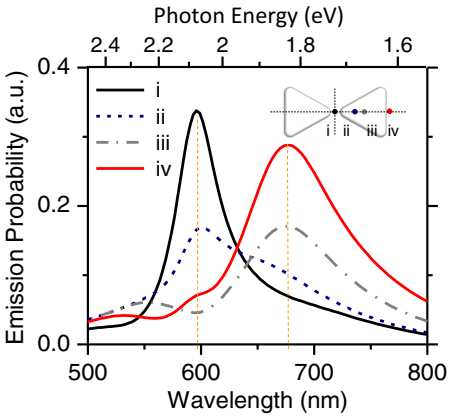

FIG. 3. (Color online) Simulated results verifying projection magnitudes of the excitation to bright and dark modes. The locations of electron beam are shown in the inset. When the electron beam is fixed at i, only the horizontal anti-parallel dipole modes can be excited (i.e., $\langle P_D|E_{\rm exc}\rangle \neq 0$ and $\langle P_B|E_{\rm exc}\rangle = 0$), which leads to a single peak close to 600 nm. As we move the electron beam from i to iv, the horizontal parallel dipole modes ($\sim$680 nm) contribute more to the projection magnitude $\langle P_B|E_{\rm exc}\rangle \neq 0$.

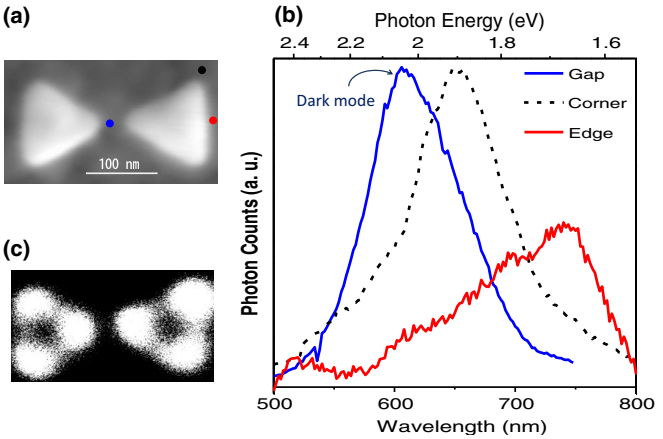

FIG. 4. (Color online) Experimentally measured scattering interaction strength at different selected locations. (a) SEM picture of a fabricated bowtie antenna. (b) Measured CL spectra at three locations indicated as colored dots in (c). Panchromatic spatial image collected for the whole spectrum detected by the photodetector. Bright color corresponds to high photon counts.

the response when the e-beam is located at the gap and the radiation from the antiparallel mode is thus the only dominant mode observed. It should be emphasized that the signal for position "i" is even higher than that of the parallel mode for position "iv," indicating a strong interaction between electron beam and photon. This is also observed in our experimental results in Sec. III B.

B. CL experiments

The gold bowtie nanoantenna was fabricated using electron-beam lithography on a multilayered substrate with minimal background luminescence and relatively low substrate index [32]. In our CL experiment, an aluminum parabolic mirror, with a small hole for electron beam, was placed on top of the sample for collecting the photons emitted by the antenna irradiated with an electron beam accelerated at 30 kV and 20 nA current. The collected photons were directed into a Mach-Czerny type monochromator to collect spectral information and imaging. Experimental setup have been previously published with details [30,32] (see Supplemental Material [33]). Our experimental results (Fig. 4) show the strong scattering interaction mediated by the dark plasmon, which agrees very much with our theory. An SEM picture of the fabricated bowtie nanoantenna is shown in Fig. 4(a). We observed three peaks for center (gap), corner, and edge excitations, indicated in the same SEM picture as blue, black, and red dots, respectively. The observation of the three modes is consistent with a previous related experiment [23]. The results [Fig. 4(b)] also agree well with the simulation results in terms of the number of peaks and relative peak positions, except the separation between peaks are larger in the experiment. The obtained peak wavelengths for center, corner, and edge excitations are, respectively, 600 nm, 650 nm, and 740 nm. We believe that the discrepancy from simulation results can be due to the detailed material and geometrical properties. The panchromatic CL image [Fig. 4(c)] also indicates that the edge excitation gives a weak signal and even the bright mode is excited.

IV. CONCLUSION

To conclude, we introduced a nontrivially strong electron-photon scattering interaction enhanced by dark plasmon modes. Our theory predicts that even though dark plasmon mode couples weakly with photon, it can strongly enhance the scattering interaction between a high energy electron and a photon. Our simulation and experiment strongly support the theoretical predictions. The discovery may offer opportunities for improving single-plasmon generation and detection in nanostructures. Our study also provides insights for developing high-resolution characterization techniques for high quality plasmonic materials. The phenomenon presented in this paper is explained by a classical model. It would be interesting to study the quantum interaction in the future.

ACKNOWLEDGMENTS

This work was supported by AFOSR MURI (Award No. FA9550-12-1-0488), National Science Foundation, the Office of Naval Research, Hong Kong RGC Grant under Early Career Scheme (Grant No. 509813), Hong Kong RGC Grant under Area of Excellence Scheme (Grant No. AoE/P-02/12), and carried out in part in the Frederick Seitz Materials Research Laboratory Central Facilities, University of Illinois, which are partially supported by the U.S. Department of Energy. We thank Chi Wai Ling for his kind help in the revision of this paper. We also thank C. T. Chan, Jun Xu, Anshuman Kumar, Hyungjin Ma, Yixin Xiao, Min Chen, and Lei Zhou for fruitful discussions.

APPENDIX A: DEGENERACY IN AN EQUILATERAL NANOTRIANGLE

Consider that an equilateral nanotriangle is driven by an external electric field $\mathbf{E}^{\text{inc}} = E_x^{\text{inc}}\hat{\mathbf{x}} + E_y^{\text{inc}}\hat{\mathbf{y}}$. We first suppose a single nanotriangle has different dipole polarizabilities for different in-plane polarizations (along x and y axes). The response dipole, $\mathbf{p} = p_x\hat{\mathbf{x}} + p_y\hat{\mathbf{y}}$, is given by

$$\begin{pmatrix} p_x \\ p_y \end{pmatrix} = \begin{pmatrix} \alpha_x & 0 \\ 0 & \alpha_y \end{pmatrix} \begin{pmatrix} E_x^{\text{inc}} \\ E_y^{\text{inc}} \end{pmatrix}, \tag{A1}$$

where p_x and p_y are the dipole moments of the nanoparticles in x and y directions, respectively. The polarizability tensor has only diagonal elements because the x and y polarization are decoupled due to a mirror symmetry along one of the axes. In addition, due to the threefold rotational symmetry, the polarizability tensor is preserved under 120° rotation:

$$\begin{pmatrix} \cos\frac{2\pi}{3} & -\sin\frac{2\pi}{3} \\ \sin\frac{2\pi}{3} & \cos\frac{2\pi}{3} \end{pmatrix} \begin{pmatrix} \alpha_x & 0 \\ 0 & \alpha_y \end{pmatrix} \begin{pmatrix} \cos\frac{2\pi}{3} & \sin\frac{2\pi}{3} \\ -\sin\frac{2\pi}{3} & \cos\frac{2\pi}{3} \end{pmatrix} = \begin{pmatrix} \alpha_x & 0 \\ 0 & \alpha_y \end{pmatrix}, \tag{A2}$$

which gives

$$\begin{pmatrix} -\sqrt{3}\alpha_x + \sqrt{3}\alpha_y & -\alpha_x + \alpha_y \\ -\alpha_x + \alpha_y & \sqrt{3}\alpha_x - \sqrt{3}\alpha_y \end{pmatrix} = \mathbf{0}, \tag{A3}$$

which implies $\alpha_x = \alpha_y$ and, therefore, the two in-plane dipole modes are degenerate. It should be noted that the degeneracy is guaranteed when we have N-fold rotational symmetry, where $N \geqslant 3$. This can be proved in a way similar to Ref. [34].

APPENDIX B: CALCULATION OF THE PROJECTION MAGNITUDE FOR ELECTRON BEAM EXCITATION

In our eigen-response theory, the electron beam is modeled as a moving point charge:

$$\begin{aligned} \mathbf{P}_{\text{exc}}(\mathbf{r}) &= -i\omega\mathbf{J}(\mathbf{r}) \\ &= i\omega ev \int e^{i\omega t}\delta^{(3)}(\mathbf{r} - \mathbf{r}_0 - \mathbf{v}t)dt\,\hat{\mathbf{z}} \\ &= i\omega\, e\delta(x - x_0, y - y_0)e^{i\omega z/v}\hat{\mathbf{z}}, \end{aligned} \tag{B1}$$

where (x_0, y_0) is the position of the electron beam. For simplicity, we evaluate the projection amplitude $\langle P_{\text{eig}}|E_{\text{exc}}\rangle$ using the reciprocity theorem. The partial projection amplitude is thus given by $\langle P_{\text{eig}}|E_{\text{exc}}\rangle = \langle P_{\text{exc}}|E_{\text{eig}}\rangle = I_1 + I_2$, where $\mathbf{E}_{\text{eig}}$ is the field produced by the eigenmode and I_1 and I_2 are the integrals for the first and the second metal nanoparticles, respectively. For x-polarized eigenmodes, the field generated by one particle on an e-beam with $y_0 = 0$ is simply given by

$$\mathbf{E}_{\text{eig},1}(z) = k_0^3 p_x \begin{pmatrix} A(k_0\sqrt{d^2+z^2}) + B(k_0\sqrt{d^2+z^2}) \\ 0 \\ B(k_0\sqrt{d^2+z^2})\frac{zd}{d^2+z^2} \end{pmatrix}, \tag{B2}$$

where $k_0 = \omega/c$, c is the speed of light in vacuum, $d = x_0 - x_d$, x_d is the x position of dipole in one nanoparticle, $A(x) = (x^{-1} + ix^{-2} - x^{-3})e^{ix}$, and $B(x) = (-x^{-1} - 3ix^{-2} + 3x^{-3})e^{ix}$. Therefore, we get

$$I_1 = i\omega p_x e k_0^3 d \int_{-\infty}^{\infty} \frac{z}{d^2+z^2} B(k_0\sqrt{d^2+z^2})e^{i\omega z/v}dz. \tag{B3}$$

I_2 can be obtained in a way similar to Eq. (B3) by using the correct displacement d.

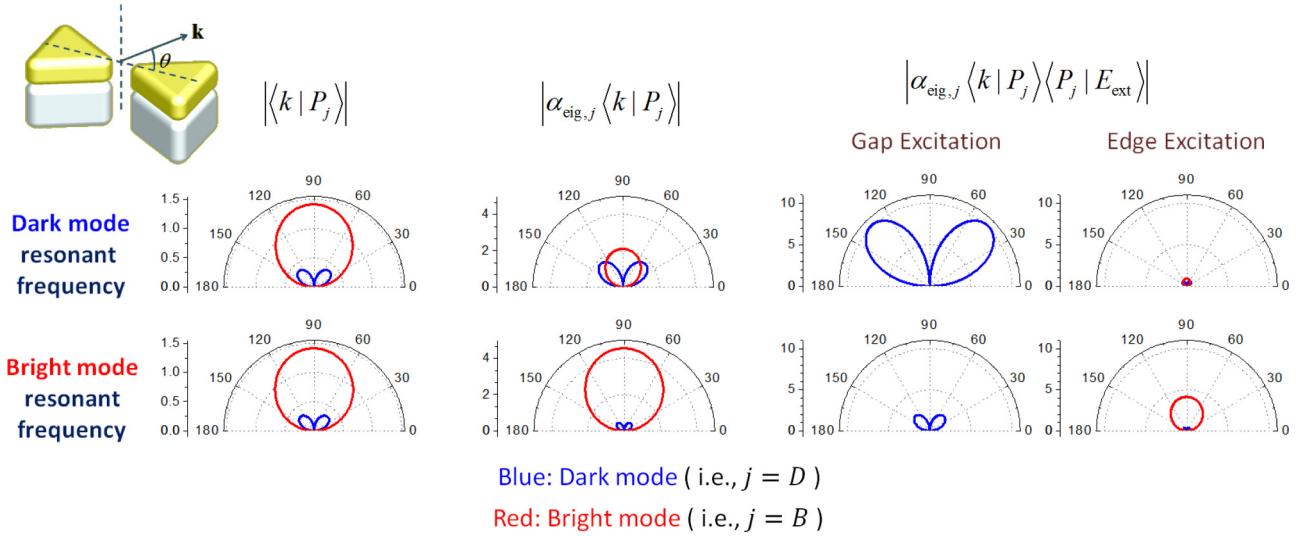

FIG. 5. (Color online) Decomposed interaction strength between electron beam and photon as a function of angle θ. Units are arbitrary. The calculation predicts that the interaction strength mediated by dark plasmon can be higher than that of the bright plasmon mode.

APPENDIX C: CONTRIBUTION OF EACH MODE TO THE TOTAL STRENGTH

Here, we evaluate the interaction strength between the electron beam and a plane wave propagating in single direction, denoted as $|k\rangle$. We evaluate the following three quantities.

(1) The interaction strength for each pure eigenmode, $|\langle k|P_j\rangle|$.

(2) The interaction strength for each pure eigenmode multiplied by the corresponding eigen-polarizability, $|\alpha_{\mathrm{eig},j}\langle k|P_j\rangle|$.

(3) The contribution of each eigenmode to the overall interaction strength, $|\alpha_{\mathrm{eig},j}\langle k|P_j\rangle\langle P_j|E_{\mathrm{ext}}\rangle|$.

Figure 5 shows that the projection plays the most important role in the final interaction strength.

APPENDIX D: MODELING OF ELECTRON BEAM

The electron beam is modeled as a moving point charge. We assume that the velocity of the electron ($\approx 0.33c$) is high enough so that its velocity does not change significantly at the time when it is close to the bowtie nanoantenna. In this case, the moving point charge can be considered as a chain of dipoles after discretization in simulation:

$$\mathbf{p}(z_m,t) = \frac{q\Delta z}{2}\mathrm{sgn}(z_m/v - t)\hat{\mathbf{z}}. \tag{D1}$$

This is equivalent to a point charge moving at a velocity v in the z direction when the dipole chain is long enough and the dipoles are dense enough (with $\Delta z \to 0$). In the frequency domain, the dipoles can be written as

$$\mathbf{p}(z_m,\omega) = \int \mathbf{p}(z_m,t)e^{i\omega t}dt = \frac{q\Delta z}{i\omega}e^{i\omega z_m/v}\hat{\mathbf{z}}. \tag{D2}$$

Instead of using the time-domain sources in Eq. (D1), we do a FDTD simulation [35] for our target structure with other time-domain sources, $\tilde{\mathbf{p}}(z_m,t) = \frac{1}{2\pi}\int \tilde{\mathbf{p}}(z_m,\omega)e^{-i\omega t}d\omega$, in which the sources in the frequency domain are renormalized with

$$\tilde{\mathbf{p}}(z_m,\omega) = i\omega s(\omega)\mathbf{p}(z_m,\omega) = q\Delta z s(\omega)e^{i\omega z_m/v}\hat{\mathbf{z}}, \tag{D3}$$

where

$$s(\omega) = \int \sin[\omega_0(t-t_0)]\exp\left(i\omega t - \frac{(t-t_0)^2}{2(\Delta t)^2}\right)dt \tag{D4}$$

and ω_0 is the pulse central frequency. The simulated CL signals are then obtained by measuring the power flow through a plane above the nanostructure. By redoing the normalizations back to the original model [Eq. (D1)], we obtained the spectral power for the dipole sources written in Eq. (D2). Since the experimental uses a uniform spectral window in wavelength instead of frequency, we further convert the numerically obtained spectral power per unit frequency to a spectral power per unit wavelength.

[1] J. N. Farahani, D. W. Pohl, H. J. Eisler, and B. Hecht, Phys. Rev. Lett. **95**, 017402 (2005).

[2] T. H. Taminiau, F. D. Stefani, F. B. Segerink, and N. F. van Hulst, Nat. Photon. **2**, 234 (2008).

[3] J. T. Choy, B. J. M. Hausmann, T. M. Babinec, I. Bulu, M. Khan, P. Maletinsky, A. Yacoby, and M. Lonèar, Nat. Photon. **5**, 738 (2011).

[4] P. Berini and I. De Leon, Nat. Photon. **6**, 16 (2012).

[5] D. J. Bergman and M. I. Stockman, Phys. Rev. Lett. **90**, 027402 (2003).

[6] M. T. Hill *et al.*, Opt. Express **17**, 11107 (2009).

[7] M. A. Noginov, G. Zhu, A. M. Belgrave, R. Bakker, V. M. Shalaev, E. E. Narimanov, S. Stout, E. Herz, T. Suteewong, and U. Wiesner, Nature (London) **460**, 1110 (2009).

[8] R. F. Oulton, V. J. Sorger, T. Zentgraf, R. M. Ma, C. Gladden, L. Dai, G. Bartal, and X. Zhang, Nature (London) **461**, 629 (2009).

[9] N. W. Bigelow, A. Vaschillo, V. Iberi, J. P. Camden, and D. J. Masiello, ACS Nano **6**, 7497 (2012).

[10] M. I. Stockman, S. V. Faleev, and D. J. Bergman, Phys. Rev. Lett. **87**, 167401 (2001).

[11] V. A. Markel, J. Opt. Soc. Am. B **12**, 1783 (1995).

[12] H. Benisty, J. Opt. Soc. Am. B **26**, 718 (2009).

[13] U. Fano, Phys. Rev. **124**, 1866 (1961).

[14] B. Luk'yanchuk, N. I. Zheludev, S. A. Maier, N. J. Halas, P. Nordlander, H. Giessen, and C. T. Chong, Nat. Mater. **9**, 707 (2010).

[15] V. Giannini, A. I. Fernández-Domínguez, Y. Sonnefraud, T. Roschuk, R. Fernández-García, and S. A. Maier, Small **6**, 2498 (2010).

[16] S. Zhang, D. A. Genov, Y. Wang, M. Liu, and X. Zhang, Phys. Rev. Lett. **101**, 047401 (2008).

[17] N. Liu, L. Langguth, T. Weiss, J. Kästel, M. Fleischhauer, T. Pfau, and H. Giessen, Nat. Mater. **8**, 758 (2009).

[18] J. B. Lassiter, H. Sobhani, J. A. Fan, J. Kundu, F. Capasso, P. Nordlander, and N. J. Halas, Nano Lett. **10**, 3184 (2010).

[19] J. A. Fan, K. Bao, C. H. Wu, J. M. Bao, R. Bardhan, N. J. Halas, V. N. Manoharan, G. Shvets, P. Nordlander, and F. Capasso, Nano Lett. **10**, 4680 (2010).

[20] P. J. Schuck, D. P. Fromm, A. Sundaramurthy, G. S. Kino, and W. E. Moerner, Phys. Rev. Lett. **94**, 017402 (2005).

[21] F. J. G. de Abajo, Rev. Mod. Phys. **82**, 209 (2010).

[22] M. W. Chu, V. Myroshnychenko, C. H. Chen, J. P. Deng, C. Y. Mouand, and F. J. G. de Abajo, Nano Lett. **9**, 399 (2009).

[23] A. L. Koh, A. I. Fernández-Domínguez, D. W. McComb, S. A. Maier, and J. K. W. Yang, Nano Lett. **11**, 1323 (2011).

[24] N. Mirsaleh-Kohan *et al.*, J. Phys. Chem. Lett. **3**, 2303 (2012).

[25] B. G. Yacobi and D. B. Holt, *Cathodoluminescence Microscopy of Inorganic Solids* (Plenum, New York, 1990).

[26] D. J. Bergman and D. Stroud, Phys. Rev. B **22**, 3527 (1980).

[27] K. H. Fung and C. T. Chan, Opt. Lett. **32**, 973 (2007).

[28] The eigenvectors here can be biorthogonal for non-Hermitian operator M.

[29] K. H. Fung and C. T. Chan, Phys. Rev. B **77**, 205423 (2008).
[30] P. Chaturvedi, K. H. Hsu, A. Kumar, K. H. Fung, J. C. Mabon, and N. X. Fang, ACS Nano **3**, 2965 (2009).
[31] See Supplemental Material at http://link.aps.org/supplemental/10.1103/PhysRevB.89.045408 for more details of the effect of rounding radius in simulation.
[32] A. Kumar, K. H. Fung, J. C. Mabon, E. Chow, and N. X. Fang, J. Vac. Sci. Technol. B **28**, C6C21 (2010).
[33] See Supplemental Material at http://link.aps.org/supplemental/10.1103/PhysRevB.89.045408 for more details of the experiment.
[34] A. MacKay, Electron. Lett. **25**, 1624 (1989).
[35] For more information, see http://www.lumerical.com/.